Synthesis, characterization, kinetic and thermodynamic investigation of silica nanoparticles and their application in mefenamic acid removal from aqueous solution

Mohammed Al-Jabari*, Imtiaz Khalid, Saleh Sulaiman, Israa Alawi, Jameleh Shilo

*Department of Chemistry, Faculty of Science, Birzeit University, Birzeit, P.O. Box 14, Ramallah, West Bank, Palestinian Authority,
Tel. 00970598238493; emails: maljabari@birzeit.edu (M. Al-Jabari), ikhalid@birzeit.edu (I. Khalid),
ssuliaman@birzeit.edu (S. Sulaiman), mhj2006_2007@yahoo.com (I Alawi), jamelehshilo96@gmail.com (J. Shilo)*

ABSTRACT

Three types of silica nanoparticles (SiO_2-ZnO(CTAB), SiO_2-(CTAB), and SiO_2-ZnO) were prepared by sol-gel method as adsorbent for mefenamic acid drug. The morphology of ZnO and silica nanoparticles were investigated using scanning and transmission electron microscopy. The results showed that the CTAB cationic surfactant and ZnO nanoparticles improved the efficiency for removing mefenamic acid from aqueous solution. The adsorption of mefenamic acid onto SiO_2-ZnO(CTAB) nanoparticles was characterized by infrared spectroscopy and the kinetic and thermodynamic adsorption mechanisms were investigated. Pseudo-first and pseudo-second-order kinetic adsorption models were applied to the adsorption of mefenamic acid onto SiO_2-ZnO(CTAB) nanoparticles. The results indicated that the experimental data fitted the pseudo-second-order model better than pseudo-first-order model. Also, the results showed that Langmuir isotherm model described efficiently the adsorption process rather than Freundlich isotherm model. The activation energy value of (74.73 kJ/mole) indicated that a chemisorption process is predominant in the adsorption mechanism due to cationic and anionic electrostatic attraction. Thermodynamic parameters of standard enthalpy, standard entropy and standard Gibbs free energy were determined at different temperatures and indicated an exothermic and spontaneous process in nature.

Keywords: Silica nanoparticles; Mefenamic acid; Adsorption; Kinetics; Thermodynamics

1. Introduction

Recently, presence and removal of recalcitrant chemical compounds in the environment has received much attention due to an incomplete elimination in wastewater treatment plants using the conventional treatment methods. As a result, residues of pharmaceuticals are still found in both surface water and wastewater [1]. Therefore it is necessary to search for other alternatives that have the ability to remove such recalcitrant compounds.

Such contamination is due to the consumption and the excretion of large quantities of pharmaceuticals via urine and faeces in wastewaters. Studies showed that even though residues of pharmaceuticals and their metabolites are usually detectable in the environment at trace levels, the low concentration level can induce toxic effects, as in the cases of antibiotics and steroids that cause resistance in natural bacterial populations [2].

Different types of adsorbents have been considered for wastewater treatment such as silica nanoparticles (SiO_2), activated carbon (AC), clay, chitosan [3–7]. Also, these adsorbents were integrated with other nanoparticles to enhance the capacity of sorption by increasing the surface area. For example, AC–ZnO nanoparticles [8,9], chitosan-zinc oxide

* Corresponding author.

nanoparticles [10], silica-SnO$_2$ [11], zero-valent iron-bentonite clay [12] and amino-silica nanoparticles [3].

Recently, mesoporous silica nanoparticles have been greatly recognized in environmental remediation especially for organic contamination due to their high melting point, high specific surface area, stable structure, controllable size (10–100 nm), biocompatibility, low toxicity and greater intrinsic reactivity of surface sites [13,14]. A cationic CTAB surfactant was used as a template to produce a highly ordered-nanomesoporous silica structure (MCM-41 type silica). This type of silica has uniform pore structure and size, and its surface can be easily functionalized for different applications [15].

Shahwan et al. [16] reported the synthesis and characterization of nano-scale zero-valent iron in the presence of kaolinite clay (nZVI-kaol) with different ratios. The synthesized nZVI-kaol materials were tested for the removal of aqueous copper, cobalt, nickel and chromium ions (Cu^{2+}, Co^{2+}, Ni^{2+} and Cr(VI), respectively) [17–24]. The adsorbents demonstrated high removal abilities toward both cations under the investigated conditions.

Sulaiman and Shahwan [25] synthesized and characterized a low-cost composite, nanoscale zero-valent iron (nZVI) immobilized on bentonite clay (B), which was prepared using the NaBH$_4$ reduction method. The B-nZVI composite was used to remove a popular non-steroidal anti-inflammatory drug mefenamic acid (MA) from aqueous solution [25].

AC-coated with ZnO nanoparticles were used for the removal of acid orange 7 and methylene blue from aqueous solution where AC-ZnO nanoparticles indicated more efficiency when compared with raw AC for the dyes removal [8]. Also, the nanocomposite chitosan-zinc oxide nanoparticles have shown to be more efficient as adsorbent for the elimination of anionic dyes [10]. Nanocomposite of silica-SnO$_2$ nanoparticles exhibited a high removal efficiency for cationic dye (methylene blue) from wastewater [11].

Recently, many studies have been published on the synthesis of functional silica nanoparticles [26]. The functionalized silica nanoparticles lead to enhance the removal efficiency. Amino-functionalized silica nanoparticles were used for removal of heavy metal ions such as Ni(II), Cd(II), Pb(II) and arsenate [27–29], while ammonium-functionalized mesoporous silica was investigated for the removal of nitrate and phosphate ions from aqueous solutions [30,31]. Also, composite of ordered mesoporous silica with graphene oxide was investigated for the removal of heavy metals from wastewater [32].

The widespread use of drugs around the world has led to increased pollution of the environment that often contaminates the water of seas and rivers, which harms human and animal health [33,34]. Mefenamic acid (MA) [(2,3-dimethyl diphenyl) amino-2-carboxylic acid], C$_{15}$H$_{15}$NO$_2$ (241.285 g/mol), shown in Fig. 1, is a popular non-steroidal anti-inflammatory agent used in treating moderate and menstrual pain [35,36]. MA is one of emerging environmental pollutants reaching the groundwater, surface water, drinking water and soil from various anthropogenic sources and is among the organic contaminants whom environmental concentrations have been greater than expected (no-effect concentration of 0.428 µg L^{-1}) [37]. A prolonged exposure to trace amount of MA can cause diarrhea, skin rash and stomach upset [38]. Since the application of
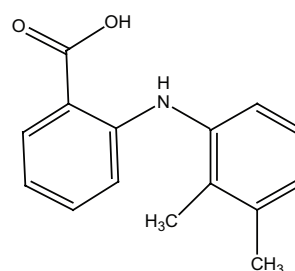
2-(2,3-dimethylphenyl)aminobenzoic acid

Fig. 1. Chemical structure of mefenamic acid (MA).

advanced treatment techniques such as membrane, adsorption or photodegradation are not sufficiently effective for MA removal from wastewater, therefore more sophisticated advanced techniques are still needed [39,40].

The goal of this study is to synthesize, characterize and investigate the adsorption potential of three types of silica nanoparticles: (SiO$_2$-ZnO(CTAB), SiO$_2$(CTAB), SiO$_2$-ZnO) for determining low concentration of MA in aqueous solution. The effect of CTAB and ZnO nanoparticles was evaluated on the adsorption capacity of mesoporous silica. Different models of the adsorption and kinetic and thermodynamic isotherms were applied to analyze the nanoparticles efficiency under different variable conditions in order to find out and understand the adsorption mechanism of MA on the surface of silica-ZnO(CTAB) nanoparticles.

2. Materials and methods

2.1. Materials

Zinc acetate dihydrate (Zn(Ac)$_2$.2H$_2$O ≥ 98%), lithium hydroxide (LiOH ≥ 98%), sodium hydroxide (NaOH ≥ 98%), ethanol ≥ 99%, ethyl acetate (EtAc ≥ 99%, tetraethyl orthosilicate (TEOS ≥ 99%), cetyltrimethylammonium bromide (CTAB ≥ 98%), mefenamic acid (MA ≥ 98.5%). Deionized water (18 ΩOhm cm). All chemicals were purchased from Sigma-Aldrich company (Germany) and were used without any further purifications.

2.2. Characterization and analysis

The absorption spectra of samples were recorded using a single beam Hp 8453 instrument which uses photodiode array detector and deuterium lamp. Fourier transform infrared (FT-IR) spectroscopy (Tensor II, Bruker, Germany) analysis was performed in the range of (4,000–200 cm^{-1}) by ATR. All the samples were analyzed in solid phase after drying. Transmission electron microscope (TEM, model JEM-2100F) and scanning electron microscope (SEM, lyra3) were used to analyze the morphology and determine the size of the nanoparticles.

2.3. ZnO nanoparticles synthesis

Synthesis of ZnO nanoparticles was carried out as described by Tang et al. [41] using 6 mg of solid LiOH. After washing, ZnO nanoparticles were dispersed in 20 mL absolute ethanol.

2.4. Silica nanoparticles synthesis

Three types of silica nanoparticles were prepared: (SiO_2-ZnO(CTAB), SiO_2-(CTAB), SiO_2-ZnO). To prepare SiO_2-ZnO (CTAB) nanoparticles, 0.2 g of CTAB was dissolved completely in 10 mL of deionized water. Then, 1 mL of ZnO nanoparticles/ethanol mixture was transferred to the solution and the resulting solution was stirred vigorously for 10 min. The resulting solution was added to a mixture of 100 mL of 13 mM NaOH solution. Then 3 mL and 1 mL of ethylacetate and TEOS were added to the aqueous solution respectively and sequentially. The reaction mixture was stirred for 3 h. The as-synthesized silica-ZnO (CTAB) nanoparticles were washed with deionized water pH 7 then with ethanol to remove the unreacted species, then the nanoparticles were dried in an oven at 60°C for 1 h. The obtained nanoparticles were kept in tightly-closed bottles for further analysis.

To prepare SiO_2-ZnO nanoparticles, same procedure was followed. After drying, the nanoparticles were dispersed in 40 mL ethanol, then the CTAB was extracted from SiO_2-ZnO (CTAB) nanoparticles by adding 80 μL of HCl (pH ~ 1.4) and the solution was stirred vigorously for 3 h at 60°C.

To prepare SiO_2-(CTAB) nanoparticles, same procedure of synthesis SiO_2-ZnO (CTAB) nanoparticles was followed with the exception that the added 1 mL of ethanol did not contain any ZnO nanoparticles.

3. Adsorption experiments

MA solution was prepared according to previous study [25]. Briefly 1,000 ppm stock solution was prepared by dissolving 1.0 g of MA in I L of deionized water adjusted to pH 8.0 using sodium hydroxide. Then, the stock solution was used to prepare the standards solutions to construct the calibration curve with concentrations in the range of 0–100 mg/L at maximum wavelength (λ) of 284 nm. All experimental samples were repeated twice and only the mean value was considered. The calibration curve was obtained with a determination coefficient (R^2) of 0.9996.

3.1. Effect of contact time

To study the removal efficiency of MA using the three types of adsorbents nanoparticles, the experiments were performed using 250 mL Erlenmeyer flasks. Deionized water was used to prepare 100 mL solutions of (10, 30 and 60 mg/L) from stock solution and 5.0 mg of adsorbents was added to each flask. The solutions were sonicated for 20 s, and the flasks were placed on a shaker for 60 min at 298 K. Samples were analyzed at different time intervals (0, 1, 2, 3, 4, 5, 10, 15, 20, 30, 40 and 60 min). At the end of the contact period, each sample was filtered using 0.45 μm membrane filters. The clear supernatant before and after adsorption was analyzed using UV–Vis spectrophotometer and the concentration of MA was determined using calibration curve. The removal efficiency of the sorbents was calculated according to Eq. (1) as follows:

$$R\left(\%\right) = \frac{C_0 - C_t}{C_0} \times 100\% \tag{1}$$

3.2. Effect of adsorbate concentration

Effect of initial MA concentrations (10, 20, 30, 40, 50 and 60 mg/L) on the adsorption was examined using 5.0 mg of SiO_2-ZnO (CTAB) nanoparticles. The 60 min contact samples were tested to ensure that the adsorption equilibrium has been reached. Then samples were analyzed at different time intervals (0, 1, 2, 3, 4, 5, 10, 15, 20, 30, 40 and 60 min).

3.3. Effect of temperature

The effect of temperature on adsorption was executed using 5.0 mg of SiO_2-ZnO (CTAB) nanoparticles in 100 mL of (30 mg/L) of MA, the sample was evaluated at three different temperatures (298, 308 and 318 K).

4. Results and discussion

4.1. Nanoparticles characterization

Surface morphology of the synthesized nanoparticles was studied using SEM and TEM techniques. Figs. 2(a) and (b) present the TEM images of ZnO nanoparticles, the images of the nanoparticles indicating average 6 nm diameter, the fringes of ZnO nanoparticles were clearly observed as presented in Fig. 2(b) and the d-spacing value around 2.4 Å which matches to the space between two (101) planes of ZnO [42]. Figs. 2(c) and (d) show the SEM and TEM images of SiO_2-ZnO (CTAB) nanoparticles, respectively. The cationic surfactant (CTAB) was used as template to produce silica nanoparticles called (MCM-41) similar to previous studies [15]. These silica nanoparticles have uniform spherical shape with 60 nm diameter. Fig. 2(d) shows the ZnO nanoparticles as dark dots attached to silica surface and between silica layers [41].

4.2. Removal efficiency

Removal efficiency of MA under three different initial concentration of MA (10, 30 and 60 mg/L) at 298 K using the three synthesized types of silica nanoparticles was evaluated. Fig. 3 shows the percentage removal efficiency of 30 ppm MA solution by three types of silica nanoparticles. The figure indicates clearly that the best performance was obtained with SiO_2-ZnO(CTAB), followed by SiO_2-CTAB, and finally with SiO_2-ZnO nanoparticles. In addition, the results indicated that the removal efficiency increases as MA concentration decreases as presented in Table 1. The adsorption equilibrium is established within 60 min, while about 90% of MA adsorption was achieved on silica nanoparticles within about one-third the equilibrium time (i.e., 20 min) for all nanoparticles used. This is due to the large surface area which was reported in previous studies ranging from 917 to 1,373 m^2 g^{-1} [43,44], and ease of accessibility of adsorbate molecules to adsorbent sites on the external surface of the silica nanoparticles.

As shown in schematic of Fig. 4, the scheme represents the proposed mechanism of the adsorption process, the attraction between positive cationic surfactant (CTAB) and negative charge of MA is the main contributor of adsorption mechanism. Another possible attraction is between ZnO nanoparticles and the MA molecules which is consistent with previous study's results [8].
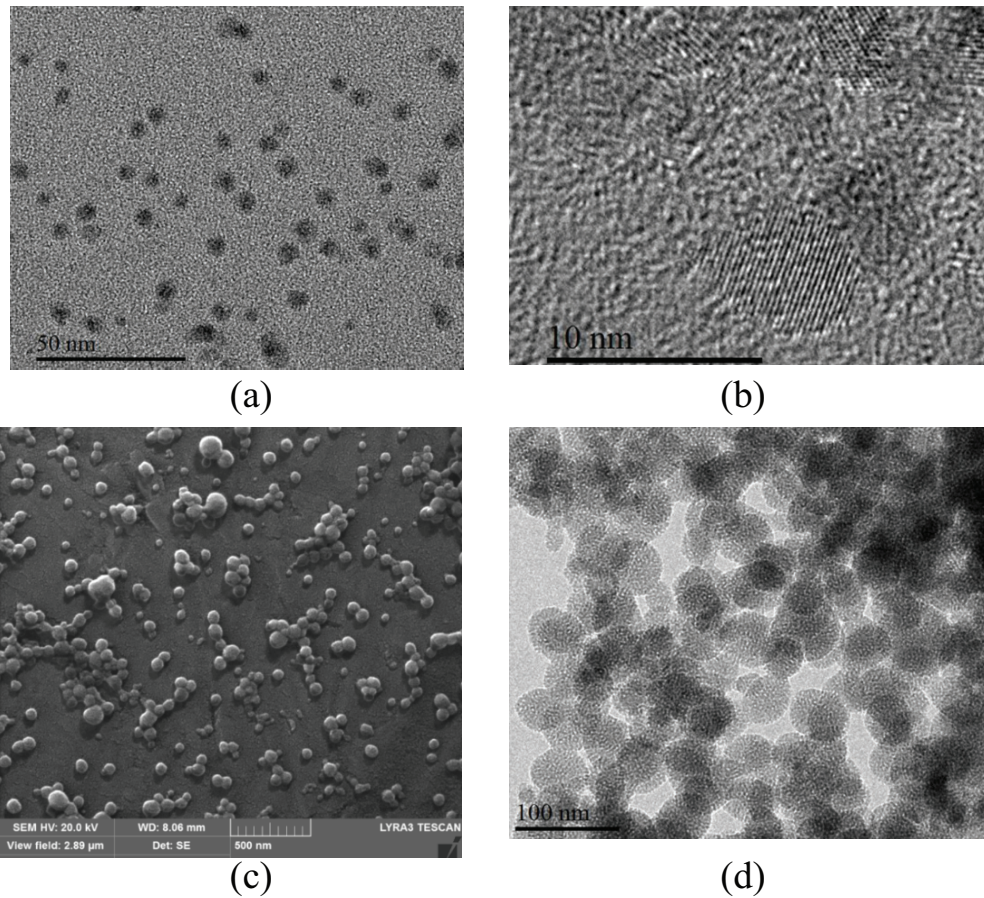
(a)

(b)

(c)

(d)

Fig. 2. ((a) and (b)) TEM images of ZnO nanoparticles, ((c) and (d)) SEM and TEM images of SiO$_2$-ZnO (CTAB) nanoparticles respectively.

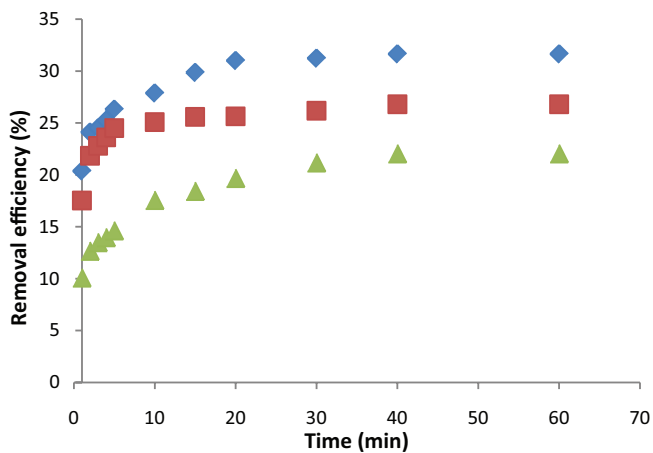Fig. 3. Percentage removal efficiency of mefenamic acid (30 mg L^{-1}) by (♦) SiO$_2$-ZnO(CTAB), (■) SiO$_2$-(CTAB), (▲) SiO$_2$-ZnO nanoparticles at 298 K.[TS: Please note that the symbols in Figs. 3 and 6 artwork should be changed to their coloured versions according to the manuscript.]

The adsorption of MA on the synthesized silica nanoparticles was characterized by FT-IR spectroscopy. Powder SiO$_2$-ZnO(CTAB) nanoparticles and MA before and after adsorption were obtained in range of 4,000–200 cm^{-1}.

Table 1
Maximum percentage removal efficiency of mefenamic acid using different types of silica nanoparticles at different initial concentrations at (298 K)

Silica nanoparticles	Maximum removal % (10 mg L^{-1})	Maximum removal % (30 mg L^{-1})	Maximum removal % (60 mg L^{-1})
SiO$_2$-ZnO(CTAB)	72.31	31.64	17.13
SiO$_2$-(CTAB)	64.11	26.81	14.69
SiO$_2$-ZnO	51.21	22.05	11.81

Figs. 5(b) and (c) show the characteristic peak at 795 cm^{-1} which is recognized due to the presence of ZnO stretching mode [45]. The IR spectra show strong peak at 444 cm^{-1} which represents the bending vibration mode of Si–O bond in silica nanoparticles. Additional strong adsorption peaks at about 1,052 cm^{-1} and 969 cm^{-1} were observed in Figs. 5(b) and (c), representing the presence of Si–O–Si stretching vibration of silanol groups.

Stretching vibrations of C–H methyl bands, can be observed at 3,970; 2,923; 2,853 cm^{-1}. Benzene ring overtone or combination bands can be observed at 2,000–1,667 cm^{-1}. C=C ring bend at 707 cm^{-1} and C=C ring stretch at 1,639 cm^{-1} as shown in Figs. 5(a) and (c). Symmetric and asymmetric

carboxylate anion CO_2^- appears at about 1,600–1,400 cm^{-1}, secondary amine N–H shows a single weak band in the 3,390–3,310 cm^{-1}, while C–N stretching band at 1,373 cm^{-1} as indicated in the spectra of Figs. 5(a) and (c). Broad peak at 3,400 cm^{-1} in spectrum (b) indicates the presence of hydroxyl group (O–H) stretch on the surface of silica nanoparticles. The peak intensity decreases after adsorption which can be related to the basic media of adsorption process (pH ≈ 8).

4.3. Adsorption kinetics

Adsorption kinetic study is important to understand the dynamic of reaction and to calculate the adsorption rate constant. The kinetic parameters are useful to provide information for designing and modeling the adsorption process [46]. Different types of kinetic and thermodynamic models describing the sorption of pollutant have been well established [47,48].

The adsorption of MA by SiO$_2$-ZnO(CTAB) nanoparticles was evaluated using pseudo-first-order and pseudo-second-order kinetic models. The linear form of pseudo-first-order kinetic model is defined according to Eq. (2) as follows:
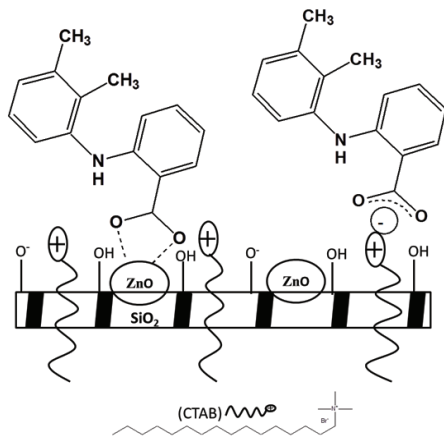
$$\ln (q_e - q_t) = \ln q_e - k_1 t \tag{2}$$

Fig. 4. Schematic representation of the adsorption of mefenamic acid on the surface of SiO$_2$-ZnO(CTAB) nanoparticles.

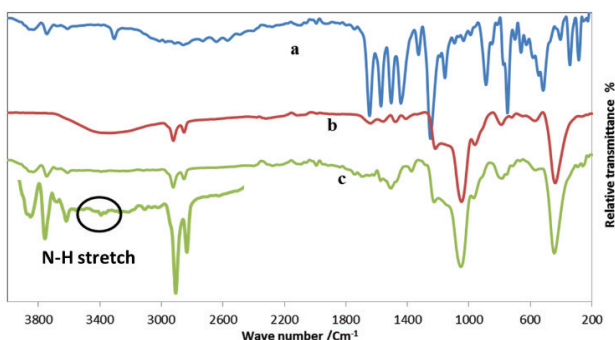Fig. 5. FT-IR spectra for (a) mefenamic acid, (b) SiO$_2$-ZnO(CTAB), (c) mefenamic acid and SiO$_2$-ZnO(CTAB).

where k_1 is the pseudo-first-order rate constant (min^{-1}), q_e is the amount of adsorbate adsorbed (µg g^{-1}) at equilibrium, q_t is the amount of adsorbate adsorbed (µg g^{-1}) at time t (min).

When this kinetic model is applicable and regression correlation coefficient value – R^2 – close to 1.0000 is obtained, then linear relationship is achieved by plotting $\ln (q_e - q_t)$ vs. t and the value of k_1 and q_e are determined from the intercept and slope of the straight line, respectively.

The linear form of pseudo-second-order kinetic model can be defined by Eq. (3) as follows:

$$\frac{t}{q_t} = \frac{1}{k_2 q_e^2} + \frac{t}{q_e} \tag{3}$$

where k_2 is the pseudo-second order rate constant (g µg^{-1} min^{-1}). If this kinetic formula is applicable, then plot t/q_t vs. t is straight line and the value of k_2 is determined.

Fig. 6 shows the pseudo-second-order model based for Eq. (3). Similarly, pseudo-first-order kinetic model was applied and the calculated parameters for the fit of pseudo-first and pseudo-second order adsorption kinetic models are summarized in Table 2. The highest value of correlation coefficient (R^2) indicates that the adsorption data fit the pseudo-second-order model better than the pseudo-first-order model. Similar results were obtained for the other types of nanoparticles at different temperatures suggesting that the rate of the adsorption process is preferably controlled by chemisorption process. Similar
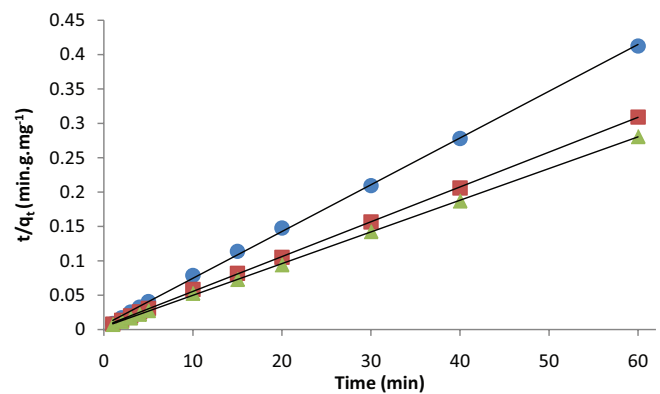

Fig. 6. Fitted pseudo-second order kinetic model for adsorption of ME by SiO$_2$-ZnO(CTAB) nanoparticles at 298 K. Initial concentrations: (●) 10 mg L^{-1}, (■) 30 mg L^{-1}, (▲) 60 mg L^{-1}.

Table 2
Kinetic parameters of pseudo-first-order and pseudo-second-order models for adsorption of different initial concentrations of MA onto SiO$_2$-ZnO(CTAB) nanoparticles

Pseudo-first-order model			Pseudo-second-order model		
C_0 (mg L^{-1})	$k_1 \times 10^2$ (min^{-1})	R^2	q_e (mg g^{-1})	$k_2 \times 10^2$ (min g mg^{-1})	R^2
10	6.430	0.9706	151.5	0.6130	0.9991
30	6.400	0.9280	200.0	0.5000	0.9995
60	6.700	0.7297	212.8	0.6130	0.9992

kinetic outcomes were obtained for adsorption of MA onto other materials such as bentonite supported by nanoscale zero-valent iron and activated charcoal [25]. Also, removal of methylene blue and acid orange 7 by activated carbon coated with ZnO nanoparticles [8], and SnO_2 quantum dots decorated silica nanoparticles for removal of cationic dye indicated similar results [11].

4.4. Adsorption isotherm

Langmuir and Freundlich are two adsorption isotherms commonly applied to describe the removal of pollutants from effluent. Langmuir model assumes monolayer adsorption on homogenous and uniform surface without attraction among the adsorbed molecules [49].

The linear relationship of the Langmuir model is presented by Eq. (4):

$$\frac{C_e}{q_e} = \frac{1}{Q_m K_L} + \frac{C_e}{Q_m} \tag{4}$$

where C_e (mg L^{-1}) is the equilibrium concentration of adsorbate (MA), Q_m (mg g^{-1}) is the complete monolayer adsorbent capacity at equilibrium, K_L (L mg^{-1}) is the Langmuir constant related to rate of adsorption.

Freundlich isotherm can be used for non-uniform or heterogeneous surface of the adsorbent [50]. The linear form of Freundlich isotherm model is given by Eq. (5):

$$\ln q_e = \ln K_F + \left(\frac{1}{n}\right) \ln C_e \tag{5}$$

where K_F (L mg^{-1}) and n (dimensionless) are Freundlich isotherm constants related to adsorption capacity and intensity, respectively. K_F and $1/n$ parameters were determined from intercept and slope of plotting $\ln q_e$ vs. $\ln C_e$, respectively.

The obtained surface heterogeneity parameter $1/n$ values are between 0 and 1. The surface becomes more heterogeneous as $1/n$ values converge to zero [51], while $1/n < 1$ indicates Langmuir isotherm [52].

If Langmuir is valid, then straight line with a slope of $1/Q_m$ is obtained when plotting C_e/q_e vs. C_e. Fig. 7 shows the well-fitted data of Langmuir isotherm model (correlation coefficient $R^2 = 0.9993$). Similar isotherm was constructed
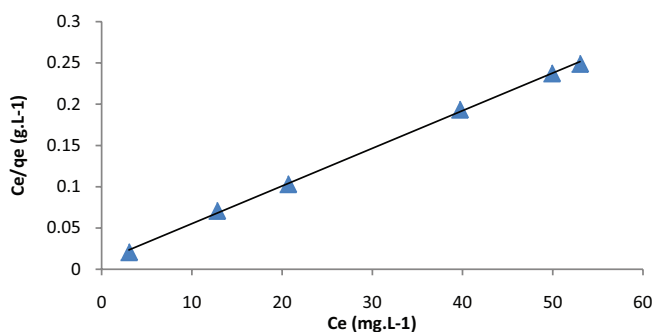
for Freundlich isotherm model at 298 K. This indicates a homogenous surface of SiO_2-ZnO(CTAB) nanoparticles, and monolayer adsorption process of MA on the surface of SiO_2-ZnO(CTAB) nanoparticles. Similar results were obtained at temperatures of 308 and 318 K.

Table 3 summarizes the kinetic isotherm parameters of Langmuir and Freundlich isotherm models. It clearly appears that the Q_m decreases at the highest temperature of 318 K. Freundlich isotherm constants $1/n$ and K_F decrease with increasing temperature. Also, $1/n$ less than unity at all temperatures indicates a normal Langmuir isotherm [53].

4.5. Effect of temperature and thermodynamic parameters

Effect of temperature change on adsorption of MA by SiO_2-ZnO(CTAB) nanoparticles was investigated at 298, 308 and 318 K. Arrhenius relation was used in order to study the activation energy of the adsorption process using Eq. (6). Other thermodynamic parameters such as heat of adsorption (standard enthalpy change $\Delta H°$), standard Gibbs free energy change of adsorption $\Delta G°$ and standard entropy change $\Delta S°$ were evaluated. The following thermodynamic equations (Eqs. (7) and (8)) were used to calculate the presented parameters.

$$\ln k_2 = \ln A - \frac{E_a}{RT} \tag{6}$$

$$\ln\left(\frac{q_e}{C_e}\right) = \frac{\Delta S°}{R} - \frac{\Delta H°}{RT} \tag{7}$$

$$\Delta G° = \Delta H° - T\Delta S° \tag{8}$$

where E_c is the activation energy (kJ mol^{-1}), k_2 is the pseudo-second-order rate constant (min g mg^{-1}), A is the pre-exponential factor, R is the gas constant (8.314 J K^{-1} mol^{-1}) and T is the temperature (K).

Values of the activation energy were evaluated from the slope of linear plot of $\ln k_2$ vs. $1/T$. The activation energy value indicates the type of adsorption; the adsorption mechanism is considered physisorption for values in the range of (5–40 kJ mol^{-1}) and chemisorption for values in the range of (40–800 kJ mol^{-1}) [54].

The activation energy for the adsorption of MA onto SiO_2-ZnO(CTAB) nanoparticles is determined to be about

Fig. 7. Langmuir isotherm of MA adsorbed by SiO_2-ZnO(CTAB) nanoparticles at 298 K.

Table 3
Langmuir and Freundlich isotherm parameters

	298 K	308 K	318 K
Langmuir isotherm			
Q_m (mg g^{-1})	217.4	217.5	138.9
K_L (L mg^{-1})	0.474	0.222	0.503
R^2	0.9993	0.9717	0.9884
Freundlich isotherm			
K_F (L mg^{-1})	134.8	126.5	112.9
$1/n$	0.121	0.102	0.039
R^2	0.9820	0.8264	0.733

Table 4
Thermodynamic parameters for the adsorption of MA ontoSiO_2-ZnO(CTAB) nanoparticles

$\Delta H°$ (kJ mol^{-1})	$\Delta S°$ (J mol^{-1})	$\Delta G°$ (kJ mol^{-1})		
		298 K	308 K	318 K
−28.89	−77.95	−5.649	−4.870	−4.090

74.73 kJ mol^{-1} indicating that the adsorption mechanism is predominantly chemisorption rather than physisorption process.

From Table 4, the negative value of enthalpy change indicates that the adsorption process was exothermic in nature, and the magnitude value of Gibbs free energy change decreases with increasing temperature meaning that the adsorption process is unfavorable at high temperature and more effective adsorption process occurs at lower temperature. Also, the negative value of $\Delta G°$ indicates that the adsorption process was spontaneous in nature, whereas the negative value of entropy change of adsorption process indicates a decrease in the degree of freedom for species in solution.

5. Conclusion

Different types of silica nanoparticles were prepared and characterized. The removal rate of MA drug from water in presence of cationic CTAB surfactant and ZnO(SiO_2-ZnO(CTAB)) nanoparticles was rapid and with high MA removal efficiency. Pseudo-second-order kinetic model is more applicable than first-order kinetic model with a correlation coefficient ($R^2 > 0.999$). The Langmuir and Freundlich isotherm models were applied with a better fitting resulting from Langmuir isotherm model. The activation energy value of 74.73 kJ mol^{-1} suggests that the adsorption is controlled by chemisorption process. Other thermodynamic parameters were evaluated such as standard enthalpy change ($\Delta H°$), standard Gibbs free energy change ($\Delta G°$), and standard entropy change ($\Delta S°$). The results clearly show an exothermic and spontaneous process in nature, and the magnitude of ($\Delta G°$) decreases with increasing temperature. Therefore, the results clearly indicate that the SiO_2-ZnO(CTAB) nanoparticles are promising for application in removal of anionic drugs or other anionic pollutants in aqueous solution.

References

[1] World Health Organization, Pharmaceuticals in Drinking Water, 2012.
[2] T.A. Ternes, R. Roman Hirsch, J. Muller, K. Haberer, Methods for the determination of neutral drugs as well as betablockers and β_2-sympathomimetics in aqueous matrices using GC/MS and LC/MS/MS, J. Anal. Chem., 362 (1998) 329–340.
[3] J. Aguado, J.M. Arsuaga, A. Arencibia, M. Lindo, V. Gascón, Aqueous heavy metals removal by adsorption on amine-functionalized mesoporous silica, J. Hazard. Mater., 163 (2009) 213–221.
[4] S. Jodeh, F. Abdelwahab, N. Jaradat, I. Warad, W. Jodeh, Adsorption of diclofenac from aqueous solution using Cyclamen persicum tubers based activated carbon (CTAC), J. Assoc. Arab Univ. Basic Appl. Sci., 20 (2016) 32–38.
[5] G. Crini, P.M. Badot, Application of chitosan, a natural aminopolysaccharide, for dye removal from aqueous solutions by adsorption processes using batch studies: a review of recent literature, Prog. Polym. Sci., 33 (2008) 399–447.
[6] S.K. Parida, S. Dash, S. Patel, B.K. Mishra, Adsorption of organic molecules on silica surface, Adv. Colloid Interface Sci., 121 (2006) 77–110.
[7] K. Kuśmierek, M. Sankowska, A. Świątkowski, Kinetic and equilibrium studies of simultaneous adsorption of monochlorophenols and chlorophenoxy herbicides on activated carbon, Desal. Wat. Treat., 52 (2014) 178–183.
[8] H. Nourmoradi, A. Ghiasvand, Z. Noorimotlagh, Removal of methylene blue and acid orange 7 from aqueous solutions by activated carbon coated with zinc oxide (ZnO) nanoparticles: equilibrium, kinetic, and thermodynamic study, Desal. Wat. Treat., 55 (2015) 252–262.
[9] V. Srivastava, D. Gusain, C.Y. Sharma, Synthesis, characterization and application of zinc oxide nanoparticles (n-ZnO), Ceram. Int., 39 (2013) 9803–9808.
[10] R. Salehi, M. Arami, N.M. Mahmoodi, Novel biocompatible composite (chitosan–zinc oxide nanoparticle): preparation, characterization and dye adsorption properties, Colloids Surf., B, 80 (2010) 86–93.
[11] D. Dutta, D. Thakur, D. Bahadur, SnO_2 quantum dots decorated silica nanoparticles for fast removal of cationic dye (methylene blue) from wastewater, Chem. Eng. J., 281 (2015) 482–490.
[12] Z.-x. Chen, X.Y. Jin, Z. Chen, M. Megharaj, R. Naidu, Removal of methyl orange from aqueous solution using bentonite-supported nanoscale zero-valent iron, J. Colloid Interface Sci., 363 (2011) 601–607.
[13] I.A. Rahman, V. Padavettan, Synthesis of silica nanoparticles by sol-gel: size-dependent properties, surface modification, and applications in silica-polymer nanocomposites-a review, J. Nanomater., 2012 (2012) 1–15.
[14] M.N. Ravi Kumar, M. Sameti, S.S. Mohapatra, X. Kong, R.F. Lockey, U. Bakowsky, G. Lindenblatt, H. Schmidt, C.M. Lehr, Cationic silica nanoparticles as gene carriers: synthesis, characterization and transfection efficiency in vitro and in vivo, J. Nanosci. Nanotechnol., 4 (2004) 876–881.
[15] T. Suteewong, H. Sai, J. Lee, M. Bradbury, T. Hyeon, M. Sol, S.M. Gruneref, U. Wiesne, Ordered mesoporous silica nanoparticles with and without embedded iron oxide nanoparticles: structure evolution during synthesis, J. Mater. Chem., 20 (2010) 7807–7814.
[16] T. Shahwan, C. Üzüm, A.E. Eroğlu, I. Lieberwirth, Synthesis and characterization of bentonite/iron nanoparticles and their application as adsorbent of cobalt ions, Appl. Clay Sci., 47 (2010) 257–262.
[17] C. Üzüm, T. Shahwan, A.E. Eroğlu, K.R. Hallam, T.B. Scott, I. Lieberwirth, Synthesis and characterization of kaolinite-supported zero-valent iron nanoparticles and their application for the removal of aqueous Cu^{2+} and Co^{2+} ions, Appl. Clay Sci., 43 (2009) 172–181.
[18] Y.C. Sharma, V. Srivastava, C.H. Weng, S.N. Upadhyay, Removal of Cr (VI) from wastewater by adsorption on iron nanoparticles, Can. J. Chem. Eng., 87 (2009) 921–929.
[19] Y.C. Sharma, V. Srivastava, Comparative studies of removal of Cr (VI) and Ni (II) from aqueous solutions by magnetic nanoparticles, J. Chem. Eng. Data, 56 (2010) 819–825.
[20] D. Gusain, F. Bux, Y.C. Sharma, Abatement of chromium by adsorption on nanocrystalline zirconia using response surface methodology, J. Mol. Liq., 197 (2014) 131–141.
[21] Y.C. Sharma, V. Srivastava, Separation of Ni (II) ions from aqueous solutions by magnetic nanoparticles, J. Chem. Eng. Data, 55 (2009) 1441–1442.
[22] V. Srivastava, Y.C. Sharma, Synthesis and characterization of Fe_3O_4@ n-SiO_2 nanoparticles from an agrowaste material and its

application for the removal of Cr(VI) from aqueous solutions, Water Air Soil Pollut., 225 (2014) 1776.

[23] V. Srivastava, Y.C. Sharma, M. Sillanpää, Application of nano-magnesso ferrite (n-MgFe$_2$O$_4$) for the removal of Co^{2+} ions from synthetic wastewater: kinetic, equilibrium and thermodynamic studies, Appl. Surf. Sci., 338 (2015) 42–54.

[24] V. Srivastava, Y.C. Sharma, M. Sillanpää, Response surface methodological approach for the optimization of adsorption process in the removal of Cr (VI) ions by Cu$_2$(OH)$_2$CO$_3$ nanoparticles, Appl. Surf. Sci., 326 (2015) 257–270.

[25] S. Sulaiman, T. Shahwan, Mefenamic acid stability and removal from wastewater using bentonite-supported nanoscale zero-valent iron and activated charcoal, Desal. Wat. Treat., 97 (2017) 175–183.

[26] B.G. Trewyn, I.I. Slowing, S. Giri, H.-T. Chen, V.S.-Y. Lin, Synthesis and functionalization of a mesoporous silica nanoparticle based on the sol–gel process and applications in controlled release, Acc. Chem. Res., 40 (2007) 846–853.

[27] X. Xin, Q. Wei, J. Yang, L. Yan, R. Feng, G. Chen, B. Du, H. Li, Highly efficient removal of heavy metal ions by amine-functionalized mesoporous Fe$_3$O$_4$ nanoparticles, Chem. Eng. J., 184 (2012) 132–140.

[28] A. Heidari, H. Younesi, Z. Mehraban, Removal of Ni (II), Cd (II), and Pb (II) from a ternary aqueous solution by amino functionalized mesoporous and nano mesoporous silica, Chem. Eng. J., 153 (2009) 70–79.

[29] H. Yoshitake, T. Yokoi, T. Tatsumi, Adsorption of chromate and arsenate by amino-functionalized MCM-41 and SBA-1, Chem. Mater., 14 (2002) 4603–4610.

[30] S. Hamoudi, R. Saad, K. Belkacemi, Adsorptive removal of phosphate and nitrate anions from aqueous solutions using ammonium-functionalized mesoporous silica, Ind. Eng. Chem. Res., 46 (2007) 8806–8812.

[31] R. Saad, K. Belkacemi, S. Hamoudi, Adsorption of phosphate and nitrate anions on ammonium-functionalized MCM-48: effects of experimental conditions, J. Colloid. Interface Sci., 311 (2007) 375–381.

[32] X. Wang, P. Yifei, L. Muxin, L. Xiaoquan, D. Xinzhen, Highly efficient adsorption of heavy metals from wastewaters by graphene oxide-ordered mesoporous silica materials, J. Mater. Sci., 50 (2015) 2113–2121.

[33] A.C. Johnson, D.J. Monika, J.W. Richard, K. Klaus, K. Andreas, P.S. John, Do cytotoxic chemotherapy drugs discharged into rivers pose a risk to the environment and human health? an overview and UK case study, J. Hydrol., 348 (2008) 167–175.

[34] J. Fick, H. Söderström, R.H. Lindberg, C. Phan, M. Tysklind, D.G. Larsson, Contamination of surface, ground, and drinking water from pharmaceutical production, Environ. Toxicol. Chem., 28 (2009) 2522–2527.

[35] T. Pringsheim, W.J. Davenport, D. Dodick, Acute treatment and prevention of menstrually related migraine headache evidence-based review, Neurology, 70 (2008) 1555–1563.

[36] R.A. Moore, S. Derry, H.J. McQuay, Single dose oral mefenamic acid for acute postoperative pain in adults. Status and date, Cochrane Database Syst. Rev., 11 (2011) 1–28.

[37] P. Chen, F.L. Wang, K. Yao, J.S. Ma, F.H. Li, W.Y. Lv, G.G. Liu, Phototransformation of mefenamic acid induced by nitrite ions in water: mechanism, toxicity, and degradation pathways, Environ. Sci. Pollut. Res., 22 (2015) 12585–12596.

[38] M. Suwalsky, M. Manrique-Moreno, J. Howe, P. Garidel, K. Brandenburg, Molecular interactions of mefenamic acid with lipid bilayers and red blood cells, J. Braz. Chem. Soc., 22 (2011) 2243–2249.

[39] M.J. Hilton, K.V. Thomas, Determination of selected human pharmaceutical compounds in effluent and surface water samples by high-performance liquid chromatography–electrospray tandem mass spectrometry, J. Chromatogr. A, 1015 (2003) 129–141.

[40] B. Soulet, A. Tauxe, J. Tarradellas, Analysis of acidic drugs in Swiss wastewaters, Intern. J. Environ. Anal. Chem., 82 (2002) 659–667.

[41] X. Tang, T. Xiaosheng, S.G.C. Eugene, L. Ling, D. Jun, X. Junmin, Synthesis of ZnO nanoparticles with tunable emission colors and their cell labeling applications, J. Chem. Mater., 22 (2010) 3383–3388.

[42] M. Mazhdi, P. Hossein Khani, Structural characterization of ZnO and ZnO: Mn nanoparticles prepared by reverse micelle method, Intern. J. Nano Dimension, 2 (2012) 233–240.

[43] Q. Cai, Z.-S. Luo, W.-Q. Pang, Y.-W. Fan, X.-H. Chen, F.-Z. Cui, Dilute solution routes to various controllable morphologies of MCM-41 silica with a basic medium, Chem. Mater., 13 (2001) 258–263.

[44] T. Suteewong, H. Sai, J. Lee, M. Bradbury, T. Hyeon, S.M. Gurner, U. Wiesner, Ordered mesoporous silica nanoparticles with and without embedded iron oxide nanoparticles: structure evolution during synthesis, J. Mater. Chem., 20 (2010) 7807–7814.

[45] J.V.G. Tinio, V.G. Jessica, A. Simfroso, V.P. Dea Marie, T.C. Rolando Jr., Influence of OH$^-$ ion concentration on the surface morphology of ZnO-SiO$_2$ nanostructure, J. Nanotechnol., 1 (2015) 1–7 (Available at: https://doi.org/10.1155/2015/686021).

[46] H. Faghihian, H. Nourmoradi, M. Shokouhi, Removal of copper (II) and nickel (II) from aqueous media using silica aerogel modified with amino propyl triethoxysilane as an adsorbent: equilibrium, kinetic, and isotherms study, Desal. Wat. Treat., 52 (2014) 305–313.

[47] Y. Ho, G. McKay, A comparison of chemisorption kinetic models applied to pollutant removal on various sorbents, Process Saf. Environ., 76 (1998) 332–340.

[48] Y.-S. Ho, G. McKay, Pseudo-second order model for sorption processes, Process Biochem., 34 (1999) 451–465.

[49] I. Langmuir, The constitution and fundamental properties of solids and liquids. Part I. Solids, J. Am. Chem. Soc., 38 (1916) 2221–2295.

[50] H. Freundlich, Over the adsorption in solution, J. Phys. Chem, 57 (1906) 1100–1107.

[51] F. Haghseresht, G. Lu, Adsorption characteristics of phenolic compounds onto coal-reject-derived adsorbents, Energy Fuels, 12 (1998) 1100–1107.

[52] K. Fytianos, E. Voudrias, E. Kokkalis, Sorption–desorption behaviour of 2, 4-dichlorophenol by marine sediments, Chemosphere, 40 (2000) 3–6.

[53] A.W. Adamson, A.P. Gast, Capillarity. Physical Chemistry of Surfaces, 6th ed., John Wiley & Sons Inc, New York, 1990, pp. 4–47.

[54] L. Cottet, C.A.P. Almeida, N. Naidek, M.F. Viante, M.C. Lopes, N.A. Debacher, Adsorption characteristics of montmorillonite clay modified with iron oxide with respect to methylene blue in aqueous media, Appl. Clay Sci., 95 (2014) 25–31.